SANDIA REPORT
SAND2008-7236
Unlimited Release
Printed November 2008

In Vivo Collection of Rare Proteins Using Kinesin-based "Nano-Harvesters"

Amanda Carroll-Portillo, Marlene Bachand, Adrienne C. Greene, and George D. Bachand

Approved for public release; further dissemination unlimited.

Sandia National Laboratories

In Vivo Collection of Rare Proteins Using Kinesin-based "Nano-Harvesters"

Amanda Carroll-Portillo, Marlene Bachand, Adrienne C. Greene, and George D. Bachand

CINT Science Department
Physical, Chemical, and Nano Sciences Center

Sandia National Laboratories
P.O. Box 5800, MS1303
Albuquerque, NM 87185-1413

Abstract

In this project, we have developed a novel platform for capturing, transport, and separating target analytes using the work harnessed from biomolecular transport systems. Nanoharvesters were constructed by co-organizing kinesin motor proteins and antibodies on a nanocrystal quantum dot (nQD) scaffold. Attachment of kinesin and antibodies to the nQD was achieved through biotin-streptavidin non-covalent bonds. Assembly of the nanoharvesters was characterized using a modified enzyme-linked immunosorbent assay (ELISA) that confirmed attachment of both proteins. Nanoharvesters selective against tumor necrosis factor-α (TNF-α) and nuclear transcription factor-κB (NF-κB) were capable of detecting target antigens at <100 ng/mL in ELISAs. A motility-based assay was subsequently developed using an antibody-sandwich approach in which the target antigen (TNF-α) formed a sandwich with the red-emitting nanoharvester and green-emitting detection nQD. In this format, successful sandwich formation resulted in a yellow emission associated with surface-bound microtubules. Step-wise analysis of sandwich formation suggested that the motility function of the kinesin motors was not adversely affected by either antigen capture or the subsequent binding of the detection nQDs. TNF-α was detected as low as ~1.5 ng/mL TNF-α, with 5.2% of the nanoharvesters successfully capturing the target analyte and detection nQDs. Overall, these results demonstrate the ability to capture target protein analytes *in vitro* using the kinesin-based nanoharvesters in nanofluidic environments. This system has direct relevance for lab-on-a-chip applications where pressure-driven or electrokinetic movement of fluids is impractical, and offers potential application for *in vivo* capture of rare proteins within the cytoplasmic domain of live cells.

Acknowledgments

Table of Contents

Figures

1.0 Introduction

Efficient transport of macromolecules within the cytoplasm is crucial to a wide range of cellular functions. The high viscosity environment limits the efficacy of diffusional transport, particularly at longer length scales such as in the axons of neurons (e.g., up to a meter in length).[1] Thus, living systems have developed a complex set of energy-consuming transport systems to achieve directed, high-efficiency transport of macromolecules within cells. These active transport systems involve specialized classes of enzymes known as motor proteins and associated cytoskeletal filaments.[2-4] For example, the motor proteins kinesin and dynein move along microtubule filaments, enabling the bi-directional transport of macromolecules, including vesicles, over considerable distances.[5] Such efficient transport systems provide useful models for understanding and engineering analogous systems in artificial nanoscale environments.

The different members of the kinesin superfamily of motor proteins are considerably diverse, but share certain conserved structural motifs: a motor domain, neck-linker domain, and often a coiled-coil tail domain (Figure 1). The motor domain of all kinesin consists of an ATP-catalytic side and a microtubule binding site.[6,7] The neck-linker domain serves as a mechanical transducer, enabling the conformational changes in protein structure needed for movement. [8-10] The coiled-coil tail domain, coupled with associated light chains, is responsible for cargo binding.[11,12] Kinesin-based transport rates of ~12 µm/sec and catalytic efficiencies (i.e., conversion of chemical energy into work) of ~50% have been reported.[13-15] All kinesin motors move along microtubules, which are hollow protein polymeric filaments with a diameter of ~25 nm and tens of microns in length. Microtubule assembly occurs through the GTP-driven polymerization of αβ tubulin dimers into protofilaments,[16] which subsequently assemble into a hollow cylinder. In cells, microtubules often polymerize from a central

Figure 1. Three-dimensional crystal structure of a conventional kinesin motor protein showing the location of the various conserved domains.

structure known as a centrosome, and form a three-dimensional transportation network within the cell.[1,17] Together, kinesin and microtubules provide a high-efficiency system for transporting macromolecular cargo through the cytoplasm of a cell.

The intriguing and powerful properties of active transport systems have spurred their application in hybrid nanoscale systems.[18-21] Early work in this area was focused on applying microfabrication technologies to guide the kinesin-based transport of molecular shuttles (i.e., stabilized microtubule filaments) and achieve directed transport of materials at the nanoscale.[22-27] In this system, known as the gliding motility geometry, kinesin motor proteins are bound on a solid surface such that their catalytic and microtubule-binding domains extend into the solution. In the presence of ATP, microtubule filaments bind to the kinesin, and guide across the surface in a highly stochastic manner.[20] As mechanisms for guiding transport emerged, work began focusing on methods of cargo attachment to molecular shuttles, and the development of simple devices and materials. The kinesin-based transport of a wide range of synthetic (e.g., metallic, semiconductor, and polymer nanoparticles)[28-32] and biological (e.g., protein, viruses, DNA, etc.)[33-39] materials on molecular shuttles has been demonstrated. More recently, the assembly of photonic nanocomposites has been achieved,[40] marking the first successful nanoscale application of kinesin transport for practical use.

The ability to transport biological materials *in vitro* using the kinesin-microtubule transport system also provides technological insight for manipulating active transport within living cells. *In vivo* control of active transport could potentially be used for studying a wide range of physiological phenomena such as axonal transport, mitotic spindle formation, chromosomal segregation, and melanophore dynamics. The central question is: can intracellular active transport systems be exploited or manipulated for specific needs? Nature has provided model systems in which pathogenic organisms have evolved the ability to "hijack" the host cell's active transport systems. For example, viruses co-opt active transport to move back and forth between the cell membrane and site of replication; the exact nature of these interactions, however, is currently unknown.[41-45] Building from this concept, the primary goal of this project was to integrate principals of *in vitro* and *in vivo* kinesin-transport to develop a system that enables the harvest of rare target proteins inside individual live cells. A key application of this technology involves the ability to capture protein analytes within a cell where their relative concentrations are considerably higher than exist after common biochemical extraction procedures. In addition, the exploitation of energy-dissipating transport (i.e., kinesin) along the three-dimensional microtubule network provides a highly efficient mechanism for probing the cytoplasmic content of a cell.
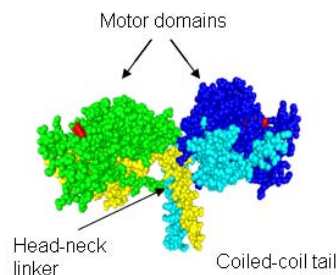
2.0   Materials & Methods

2.1 Kinesin construction

A histidine-tagged (His-tag), biotinylated kinesin was developed based on the K401-bio plasmid, which contains the first 410 amino acids of a conventional kinesin from *Drosophila melanogaster* and the biotin-carboxyl carrier proteins (BCCP) immediately downstream. The base plasmid (K401-bio) was generously provided by Dr. Jeff Gelles at Brandeis University. Two oligomers were commercially synthesized to introduce the 10x His-tag (sequenced underlined) into the K401-bio plasmid:

His-For: 5'-AATTCGACGAACCGCTTGTTGTTATCGAA<u>CACCATCACCATCACCATCACCATCACCAT</u>TAAA-3'
His-Rev: 5'-TTTA<u>ATGGTGATGGTGATGGTGATGGTGATGGTG</u>TTCGATAACAACAAGCGGTTCGTCGAATT-3'

The K401-bio plasmid was double digested with *EcoR*I and *Hind*III restriction endonucleases to create sticky ends for ligation of the oligomers. The digested plasmid was separated on an agarose gel, and a corresponding 3880-bp DNA bands was excised and column purified. The oligomers were then ligated into the digested plasmid using the Clonables™ 2x Ligation Premix (Novagen, Inc.), and incubation at 16°C for 15 min. The resulting reaction was then transformed into NovaBlue competent cells (Novagen, Inc.), and plated on selective media and grown overnight at 37°C. Several colonies were selected, and plasmid DNA was isolated and sent for sequencing to confirm successful insertion of the 10x His-tag. Once confirmed, the plasmid was transferred and expressed in *Escherichia coli* BL21(DE3)pLysS competent cells (Stratagene Corp.) as previously described.[46] The recombinant K401-bio-His motors were purified using Ni-NTA sepharose chromatography as previously described.[28,46] Purified protein was confirmed by SDS-PAGE electrophoresis, and stored in small aliquots at -80°C until nanoharvester construction.

2.2 Nanoharvester assembly and validation

<u>Nanoharvester construction</u>

"Nanohavesters" (Figure 2) were constructed using streptavidin-coated nanocrystal quantum dots (nQDs) as a scaffold for spatially co-organizing biotinylated kinesin (motor transport component) and biotinylated antibodies (analyte capture component). Qdot® 605 or 655 (Invitrogen Corp.) nQDs were used for constructing all nanoharvesters in these experiments. Each nQD possesses 5-10 streptavidin molecules on the surface, corresponding to 20-40 available biotin-binding sites (assuming all are active and available).

Nanoharvesters were assembled by preparing a solution containing 50 nM nQDs, 350 nM biotinylated kinesin, and 150 nM biotinylated antibody in BRB80 (80 mM PIPES pH 6.9, 1 mM

Figure 2. Nanoharvesters were constructed through attachment of biotinylated kinesin and antibodies on streptavidin-coated nanocrystal quantum dots (nQDs).

MgCl$_2$, 1mM EGTA) containing 1 mM ATP. Under these conditions, each nanoharvester should possess an average of seven kinesin motors and three antibodies per nQD. The ratios of motors and antibodies were varied to optimize function as described below. The nanoharvester solution was then incubated on rotator at room temperature for 30 – 60 min.

<u>Validating nanoharvester assembly</u>

A modified version of an enzyme-linked immunosorbent assays was used to confirm assembly of the nanoharvesters. The assay involved attachment of specific protein analytes to a microtiter plate, followed by introduction of the nanoharvesters. Once unbound nanoharvesters were removed, an enzyme-conjugated anti-kinesin antibody was added and used to detect the presence of the motors. Thus, a colorimetric change in the substrate would only be achieved if both the kinesin motors and antibodies were co-organized on the nQDs.

Microtiter plates (Nunc MaxiSorp 96) were coated with varying concentrations of either tumor necrosis factor-α (TNF-α) or nuclear transcription factor-κB (NF-κB): 1000 µg/mL, 500 ng/mL, 100 ng/mL, 10 ng/mL, 1ng/mL, 100 pg/mL, and 0 ng/mL (control). All TNF-α and NF-κB solutions were prepared in bicarbonate/carbonate coating buffer pH 9.6, and incubated at 37°C for 3 hr. Plates were then washed twice with PBST (PBS+ 0.05% Tween-20)

for 3 min each, and blocked for 1 hr at room temperature with PBST containing 1% BSA. Nanohavesters selective against either TNF-α or NF-κB were then added to the plates, and incubated overnight at 4°C. Plates were then washed three times with PB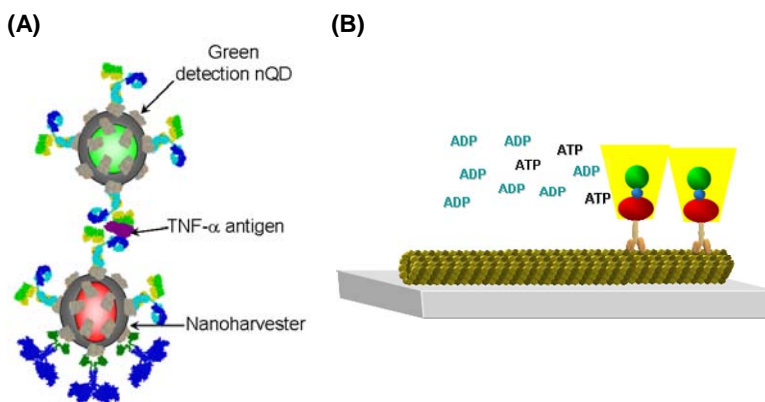ST for 3 min each, followed by the addition of an alkaline phosphatase-conjugated anti-kinesin antibody. Following a 3 hr incubation at 37°C, plates were washed three times with PBST, and the substrate (PNPP) was added to each well. The absorbance at 405 nm of each well was measured at 60 and 90 min after substrate addition.

2.3 Optimizing nanoharvesters properties

Optimization of the nanoharvesters involved varying the number of kinesin motors and antibodies per nQD to achieve maximum motor function and antigen capture, respectively. The number of motors necessary to achieve optimal transport of nQDs was determined for each lot of purified biotinylated kinesin and different size nQDs (e.g., Qdot® 605 and 655). Kinesin-based transport was evaluated using the normal motility assay,[47,48] in which kinesin motors move along taxol-stabilized microtubules that are bound to functionalized glass surfaces. Fluorescence microtubules were polymerized at 37°C for 20 min using a mixture of unlabeled and rhodamine-labeled tubulin prepared in GPEM (80 mM PIPES pH 6.9, 1 mM MgCl$_2$, 1mM EGTA, 100 mM GTP, and 5% glycerol). Microtubules were then stabilized by diluting 100-fold into BRB80T (BRB80 with 10 μM paclitaxel). Coverslips were prepared using 25 x 25 mm cover glass slips (VWR) cleaned by UV ozone for 20 minutes, and then functionalized with APDEMS (aminopropylsilanetriol 22-25% in water) and baked at 100°C for 20 min in a vacuum chamber. Standard flow cells were then assembled with the APDEMS coverslips, glass slides and double-sided tape. Polymerized microtubules were diluted in BRB12T (12 mM PIPES pH 6.9, 1 mM MgCl$_2$, 1mM EGTA, and 10μM Taxol) supplemented with 0.2 mg/mL casein, 1mM ATP and an oxygen-scavenging system (0.008 mg/mL catalase, 0.02 mg/mL glucose oxidase, 20 mM D-glucose, and 1 mM DTT). The microtubules were introduced to the flow cell and incubated for 10 min at room temperature. The flow cell was then blocked with BRB12CAT (BRB12T, 1 mM ATP, and 5 mg/mL casein) for 10 min. Kinesin-coated nQDs were prepared as described above for the nanoharvesters. For initial optimization of kinesin motors, no antibodies were used in nanoharvester assembly and the number of kinesin per nQD was systematically varied from 1 – 10 motors. The number of antibodies was then systematically varied from 0 – 10 antibodies per nQD to optimize nanoharvesters function. Kinesin-nQDs or complete nanoharvesters were introduced to the flow, incubated for 5 min, and then characterized using fluorescence microscopy. Time-lapse images of kinesin-nQDs were collected, and processed using Olympus Microsuite software. The velocity, binding, and percent nQDs moving were evaluated for each treatment.

2.4 In vitro capture and detection

In vitro capture and detection of TNF-α by nanoharvesters was performed using the normal motility as described above. Flow cells were constructed using APDEMS-coated coverslips, rhodamine microtubules were bound to the surface, and flow cells were blocked with BRB12 with 5 mg/mL casein. Nanoharvesters were constructed with seven kinesin motors and three antibodies per nQD (Qdot®655) in BRB12CAT (BRB12 with 0.2 mg/mL casein, 1 mM ATP and 10 μM paclitaxel), and stored at 4°C. TNF-α was then added to a final concentration of 165 ng/mL, and incubated at 4°C. Secondary, detection nQDs (streptavidin-coated Qdot®525) were assembled in a solution containing 2.5 nM nQDs, and

Figure 3. (**A**) The in vitro capture and detection assay involved the formation of a "sandwich" between the nanoharvesters (red nQD) and a detection nQD (green) only in the presence of the target analyte. (**B**) Movement of the sandwiched nQDs was detected by yellow fluorescence (combined red and green emission) along microtubule filaments bound to a surface.

75 nM biotinylated anti-TNF-α in BRB12CAT. The secondary nQDs were incubated for 5 – 10 min at 4°C, and then added to the reaction containing the nanoharvesters and antigen. An antibody "sandwich" between the two nQDs

(red and green) should form only in the presence of the antigen, as shown in Figure 3A. Following incubation, the complete mixture was added to the flow cell and characterized by fluorescence microscopy. The presence of yellow fluorescence (combined red and green) indicated the successful capture of TNF-α (Figure 3B). Time-lapse images of kinesin-nQDs were collected, and processed using Olympus Microsuite software. The velocity, binding, and percent nQDs moving were evaluated for each treatment. To evaluate the sensitivity of TNF-α detection, nanoharvesters were exposed to varying dilution of antigen: 0, 1.65, 16.5, 82.5, 165, and 205 ng/mL. Time-lapse images were collected, and analyzed as described above.

3.0   Results and Discussion

3.1 Biotinylated, His-tag kinesin construction

A 10x His tag was inserted at the C-terminus of the biotin carboxyl carrier protein domain (BCCP) in order to facilitate purification of the K401-bio kinesin motor protein (Figure 4). DNA sequencing confirmed insertion of the 10x His tag into the plasmid. The confirmed plasmid was transformed and expressed in *E. coli* BL21(DE3) pLysS, and the recombinant K401-bio-His kinesin was purified by Ni-NTA affinity chromatography. Because a portion of the BCCP gene was removed during insertion of the His tag, the level of biotinylation was measured to ensure that the protein was efficiently labeled. The level of kinesin biotinylation was >70% for all preparations used for nanoharvester assembly. Based on the results from the normal motility assays, the recombinant kinesin was active for 2 – 3 weeks when stored at -80C.
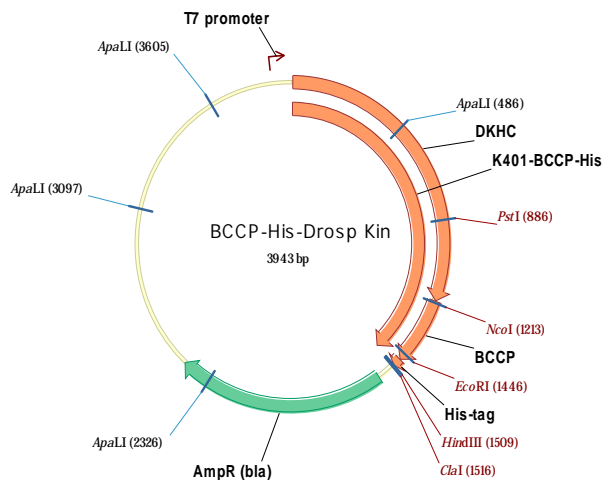
Figure 4. Plasmid map of the constructed K401-bio-His kinesin motor protein.

3.2 Assembly and optimization of nanoharvesters

The ELISA-based assays demonstrated successful assembly of nanoharvesters selective against both TNF-α and NF-κB (Figure 5). For both analytes, the absorbance at 405 nm followed an exponential rise to a maximum across the concentration range tested, as expected in these assays. The absorbance was generally lower for NF-κB than TNF-α, which may be due to the efficacy of antibody binding the nQDs. The anti-NF-κB antibody was biotinylated
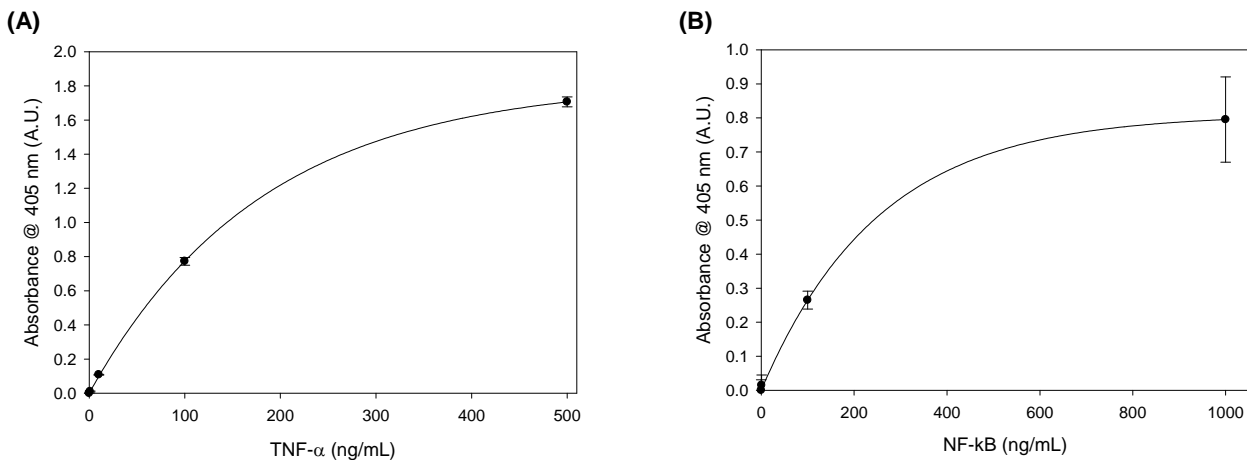
Figure 5. Results from ELISA-based assays confirming the successful assembly of nanoharvesters selective against TNF-α (**A**) and NF-κB (**B**). Values are mean ± standard error of the mean.

in our lab, whereas the anti-TNF-α antibody was purchased already biotinylated. Thus, the level of biotinylation of the anti-NF-κB may have been lower, resulting in less attachment to the nanoharvesters. The sensitivity of detecting both analytes was between 10 and 100 ng/mL in these assays. Overall, these ELISAs demonstrate successful assembly of the nanoharvesters.

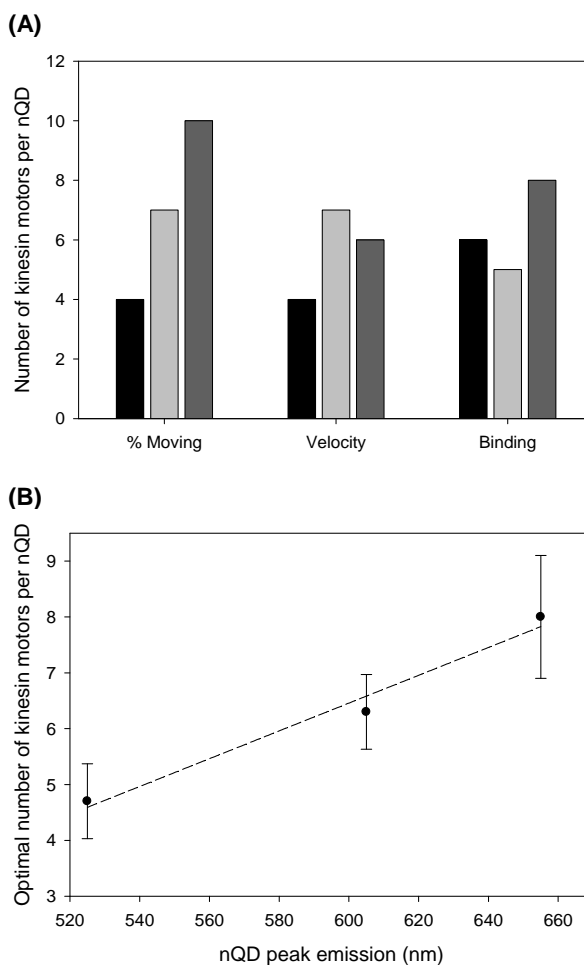The functional properties of the nanoharvesters were optimized by first varying the density of kinesin motors as a function of the different quantum dots. The number of motors required per nQD to achieve quantum dot movement increased linearly based on the size of the quantum dot (Figure 6A), while the velocity and binding of nQDs per field of view showed little size dependency. The independent relationship between motor density and velocity/binding of kinesin-coated polymer beads has previously been demonstrated.[49] The values from the three measured parameters were averaged (equal weight for each parameter) to determine the conditions for optimal function (Figure 6B). Overall, the optimal number of kinesin motors per nQD displayed a linear relationship to the nQD peak emission, which directly correlates with size.

Nanoharvesters were then optimized with respect to the ratio of kinesin motors and antibodies per nQD. The effect of antibody-coupling to the kinesin-coated nQD (i.e., the complete nanoharvesters) was then evaluated by varying the ratio from 0 – 10 (10:0, 10:3, 10:5, and 10:9) antibodies per nQD. The binding of nanoharvesters per field of view was similar at the ratios of 10:0, 10:5, and 10:9, but significantly lower for the 10:3 ratio of kinesin to antibodies (Figure 7A). This observed difference was attributed to less non-specific binding of nanoharvesters to the APDEMS surface. The velocity of the nanoharvesters was significantly affected only at the 10:9 ratio of kinesin to antibodies (Figure 7B), which is likely due to either steric crowding of the kinesin motors by the antibodies, or competition for available streptavidin sites. The velocity observed at the other ratios was ~0.5 μm/sec, which is consistent with previous reports.[47,48,50] The percentage of functional nanoharvesters was greatest at the 10:3 ratio, and lowest at the 10:9 ratio (Figure 7C). Based on these data, the three antibodies per nQD was selected as the optimal conditions for nanoharvester functionality.

(A)

(B)

Figure 6. (**A**) The number of kinesin motors per nQD required to attain maximum quantum dot movement (i.e., % quantum dots moving per field of view), velocity, and binding per field of view for Qdot® 525 (black bar), Qdot® 605 (light gray bar), and Qdot® 655 (dark bar). (**B**) The numbers of motors per nQD for each treatment were averaged (equal weight to each parameter) to provide an estimate for the optimal conditions for each size nQD. The data followed an approximate linear relationship. Values are mean ± standard error of the mean.

3.3 In vitro *capture and detection*

The ability of kinesin nanoharvester to capture, transport, and detect target analytes *in vitro* was evaluated using a sandwich-based approach in the normal motility assay. In this approach, the target antigen is captured by the nanoharvesters (red nQD), and forms a sandwich with a detection (green) nQD (Figure 3A). The co-localization of red- and green-emitting nQDs in the sandwich results in a yellow fluorescence signal that moves along microtubules in the normal motility assay.

The ability of the nanohavesters to capture and transport TNF-α was initially evaluated in a step-wise manner. Nanohavesters were assembled using red quantum dots (e.g., Qdot® 655) and a monoclonal antibody selective against TNF-α, as described above. Secondary, green nQDs coated with polyclonal anti-TNF-α antibody were prepared as described above. Three separate treatments, representing each step in the sandwich formation, were prepared: (1) nanoharvesters alone, (2) nanoharvesters with 165 ng/mL TNF-α, and (3) nanohavesters with 165 ng/mL TNF-α and secondary detection nQDs. Each treatment was introduced to separate flow cells, incubated for 10 min, and imaged by fluorescence microscopy.

Nanoharvesters were able to successfully capture and transport TNF-α in motility assays (Figure 8). Yellow fluorescence from nano-harvester sandwiches was observed to move along microtubules; blinking of the nQDs also confirmed the co-localization of the two nQDs. The average velocity over all treatments was ~0.40 ± 0.02 μm/sec, and did not significantly vary based on treatment (P = 0.129; Figure 9). The percent movement of nanoharvesters did, however, vary significantly based on the different treatments (P < 0.001; Figure 9). The percent nanoharvester movement in the complete sandwich assay was significantly lower than the nano-harvesters alone. This observation may be due to non-specific binding of the detection nQDs either to the microtubules or the APDEMS-coated surface. A significant percentage (~8%) of nano-harvesters with captured analyte and secondary nQDs moved in each field of view. In addition, isolated instances (<1%) of green nQDs (not coupled to red nQDs) moving along microtubules was observed, suggesting that free biotinylated kinesin motors were capable of binding to open streptavidin sites on the green nQDs. While such events did not affect the assay, covalent coupling of antibodies to detection nQDs represents a potential route for eliminating the unintended binding of motors to detection nQDs.

The sensitivity and selectivity of the nanoharvesters was next tested using a dilution series of TNF-α (0 – 205 ng/mL. Approximately 5% of the nanoharvesters per field of view (FOV), as detected by the binding of a green detection nQD, successfully captured TNF-α antigen across all concentrations of TNF-α evaluated. The level of detection as a function of TNF-α concentration was non-linear, and varied significantly based on concentration (P < 0.001; Figure 10A). Non-specific sandwich formation (2.4 ± 0.4%) was observed in the absence of TNF-α, and likely due
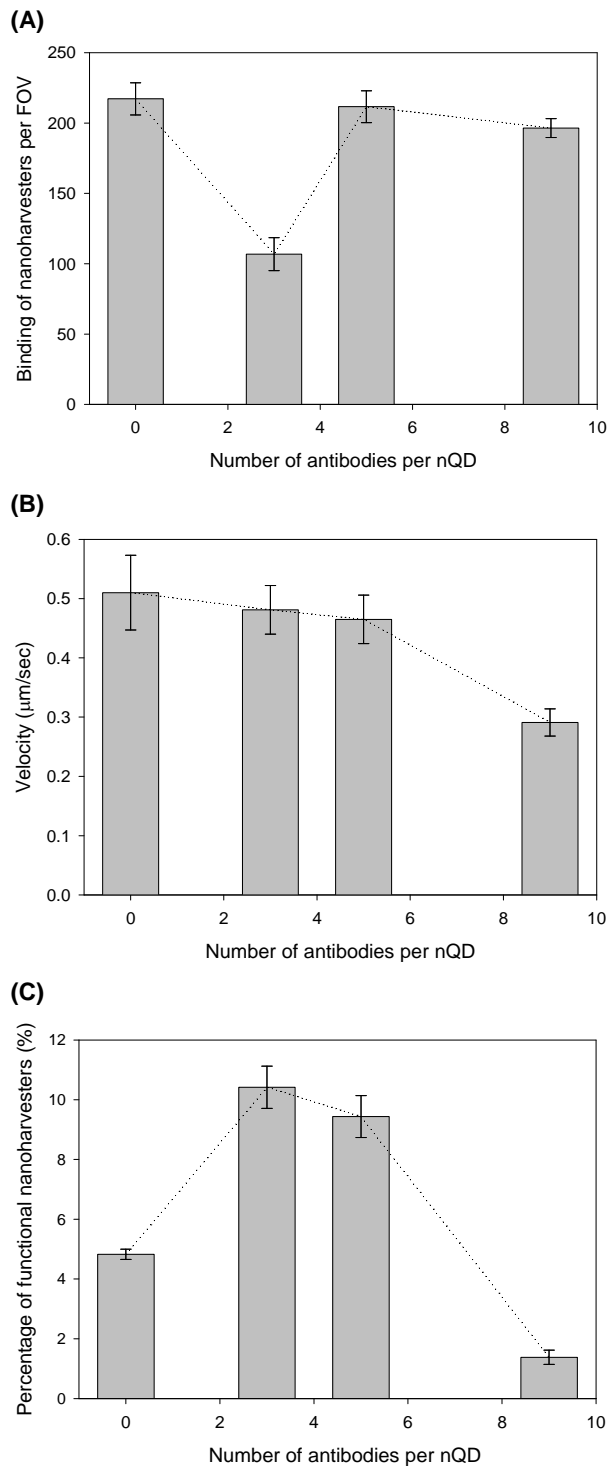
Figure 7. The binding of nanoharvesters per field of view (**A**), velocity (**B**), and percentage of functional nanoharvesters (**C**) for the varying ratios of kinesin to antibodies. Dotted lines were added to help visualize trends in each parameter as a function of increasing numbers of antibodies per nQD. Bars are mean ± standard error of the mean.
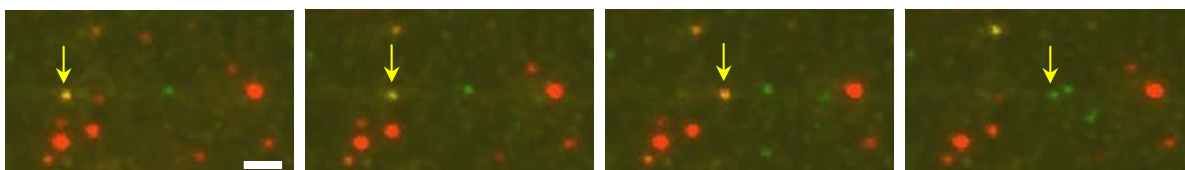
Figure 8. Time-lapse photomicrographs showing the capture and transport of TNF-α by kinesin nanoharvesters. Yellow fluorescence is observed when a "sandwich" is formed by antibody-functionalized red and green nQDs bound together in the presence of TNF-α. Blinking of the nQDs over time can be observed and enables the signal of each nQD to be confirmed. Yellow arrows are used to mark movement of harvester between frames. Images represent 5 sec intervals. Scale bar = 2 µm.

to the cross-reactivity of the two streptavidin-coated nQDs with biotinylated antibodies. As discussed above, covalent linking of antibodies to the detection nQD may alleviate this issue. The percentages of nanoharvesters with captures for all TNF-α concentration were significantly greater than the level of non-specific binding (P <0.001), suggesting that the sensitivity of detection was at ~1.65 ng/mL (P = 0.006; comparison with negative control). The greatest level of detection (11%) was observed at the 16.5 ng/mL concentration of TNF-α, and decreased at the higher concentrations. This decrease is likely a result of competition between TNF-α bound to the nanoharvesters and in free solution for antibody sites on the detection nQDs. At high concentrations, free TNF-α can bind directly to the detection nQD and limit binding to the TNF-α bound to the nanoharvesters. This issue (i.e., analyte competition) should be carefully considered when designing *in vitro* diagnostic systems in order to maximize detection across a broad range of analyte concentrations. Removal of unbound analytes prior to introduction of the detection nQDs represents one potential mechanism to alleviate competition and optimize detection.

The mean velocity of nanoharvesters with captures (i.e., antigen and detection nQDs) was 0.28 ± 0.03 µm/sec, and varied significantly across the different concentrations (Figure 10B; P = 0.02). The velocity of nanoharvesters with captures at the 16.5 (0.37 ± 0.05 µm/sec) and 82.5 (0.41 ± 0.09 µm/sec) ng/mL concentrations were similar to those observed in initial assays (Figure 8). A significant decrease in velocity, however, was observed at the 1.65 ng/mL concentration of TNF-α, but within the normal range expected.[48,50] Together these data suggest that kinesin-based transport was not adversely affected by the capture of TNF-α or presence of detection nQDs. Thus, the sandwich approach may be successfully applied to lab-on-a-chip applications in which kinesin transport is used to capture and separate target analytes from a mixed solution.

The percentage of moving nanoharvesters with captures (i.e., antigen and detection nQDs) was 18 ± 1.6%, and did not vary across the different TNF-α concentrations (P = 0.545; Figure 10C). Overall, the percentage of nanoharvesters with captures moving was similar, within experimental variation, to that observed in the step-wise evaluation of nanoharvester movement (Figure 9).

Overall, these experiments demonstrate the successful development of an *in vitro* diagnostic assay using kinesin-based nanoharvesters. The primary advantage of this technology involves the application of nanoscale, biomolecular transport to actively shuttle captured analytes within the confines of a device. This system offers a unique paradigm in which analytes are moved within a static medium. Such a system removes the need for mechanical pumping or electrokinetic-driven flow of analytes for diagnostic analysis. Rather, the conversion of chemical energy into mechanical work by kinesin motors proteins is used to actively capture,
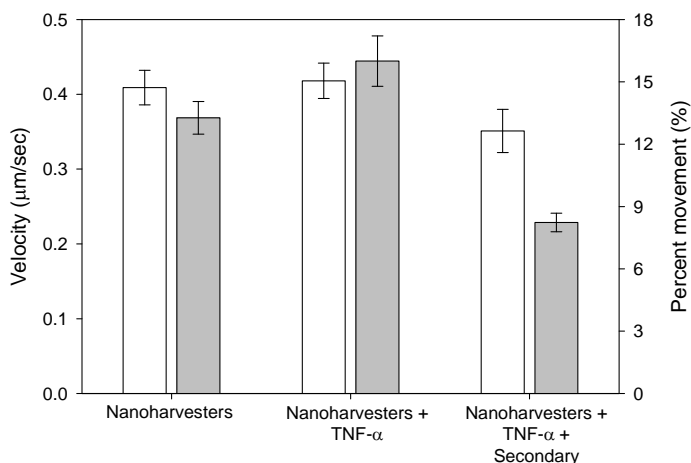

Figure 9. Transport velocity (white bars) and percent movement (gray bars) of nanohavesters alone, nanoharvesters with TNF-α, and the complete sandwich assay (i.e., nanoharvesters with TNF-α, and secondary detection nQDs). Bars are mean ± standard error of the mean.

`transport, and separate target analytes within a solution. The efficiency of the chemo-mechanical conversion is ~50%, and makes it an attractive means of accomplishing nanofluidic transport in lab-on-a-chip devices.

4.0 Conclusions

We have demonstrated the ability to apply biomolecular transport for the *in vitro* capture and transport of target analytes. In contrast to previous work,[33,39] this system uses nQDs co-functionalized with kinesin and antibodies (i.e., nanoharvester) to capture and transport protein analytes in the normal motility geometry. Assembly of nanoharvesters selective against TNF-α and NF-κB was confirmed using an ELISA-based method, and demonstrates the ability to assemble nanoharvesters against a range of target analytes. Detection of captured analytes in motility assays was accomplished using a secondary nQD with a different spectral emission to form an antibody-based sandwich. TNF-α was successfully detected at levels as low as 1.65 ng/mL, and did not adversely affect the motility function of the kinesin motors. Overall this system offers tremendous applications in lab-on-a-chip applications based on the ability to harness useful work from the biomolecular conversion of chemical energy into mechanical work. This work can be used to actively capture, transport, and separate target analytes in the absence of pressure-driven or electrokinetic flow. This system may also be adapted for *in vivo* capture of analytes within the cytoplasm of a cell. The ability of kinesin-coated nQDs to move along the microtubule networks of live cells has previously been demonstrated.[50] By applying a similar strategy, kinesin-based nanoharvesters may be introduced into live cells and used to capture analytes within the confines of a cell where the effective concentration of analytes is much greater than following traditional extraction procedures. If successful, nanoharvesters may be used to capture rare target proteins within cells, and study physiological phenomena such as innate immunity in a manner not achievable by current methods.
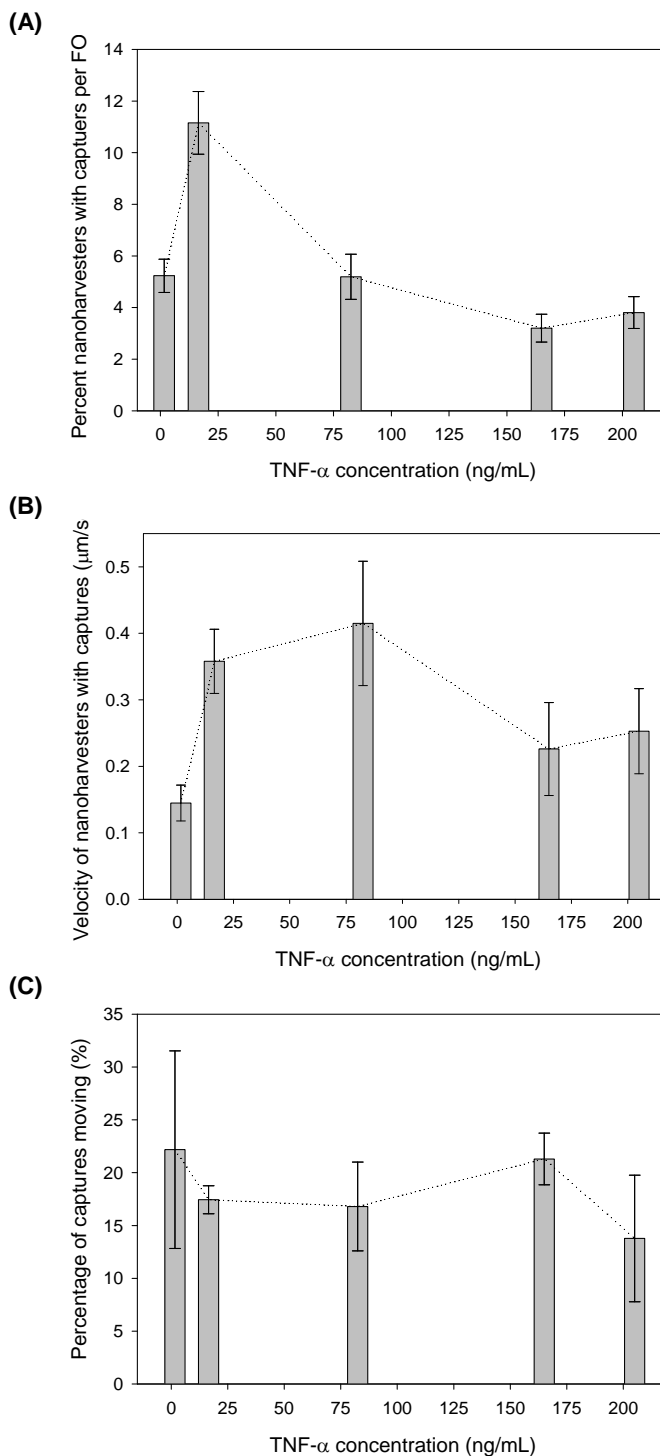
Figure 10. The percent of nanoharvesters with captures per field of view (**A**), velocity of nanohavesters with captures (**B**), and percent of captures moving (**C**) as a function of TNF-α concentration. Dotted lines were added to help visualize trends over the different concentrations. Bars are mean ± standard error of the mean.

5.0   References

1. Howard, J., *Mechanics of motor proteins and the cytoskeleton*. (Sinauer Associates, Inc., Sunderland, 2001).
2. Goldstein, L.S.B. and Philp, A.V., The road less traveled: Emerging principles of kinesin motor utilization. *Annu. Rev. Cell Dev. Biol.* **15**, 141 (1999).
3. Vale, R.D. and Fletterick, R.J., The design plan of kinesin motors. *Annu. Rev. Cell Dev. Biol.* **13**, 745 (1997).
4. Goldstein, L.S.B. and Yang, Z.H., Microtubule-based transport systems in neurons: The roles of kinesins and dyneins. *Annu. Rev. Neurosci.* **23**, 39 (2000).
5. Howard, J., The movement of kinesin along microtubules. *Annu. Rev. Physiol.* **58**, 703 (1996).
6. Huang, T.G. and Hackney, D.D., Drosophila kinesin minimal motor domain expressed in *Escherichia coli* - Purification and kinetic characterization. *J. Biol. Chem.* **269**, 16493 (1994).
7. Rivera, S.B., Koch, S.J., Bauer, J.M., Edwards, J.M., and Bachand, G.D., Temperature dependent properties of a kinesin-3 motor protein from *Thermomyces lanuginosus*. *Fungal Genet. Biol.* **44**, 1170 (2007).
8. Schief, V.R. and Howard, O., Conformational changes during kinesin motility. *Curr. Opin. Chem. Biol.* **13**, 19 (2001).
9. Tomishige, M. and Vale, R.D., Controlling kinesin by reversible disulfide cross-linking: Identifying the motility-producing conformational change. *J. Cell. Biol.* **151**, 1081 (2000).
10. Case, R.B., Rice, S., Hart, C.L., Ly, B., and Vale, R.D., Role of the kinesin neck linker and catalytic core in microtubule-based motility. *Curr. Biol.* **10**, 157 (2000).
11. Manning, B.D. and Snyder, M., Drivers and passengers wanted! The role of kinesin-associated proteins. *Trends Cell Biol.* **10**, 281 (2000).
12. Seiler, S., Kirchner, J., Horn, C., Kallipolitou, A., Woehlke, G., and Schliwa, M., Cargo binding and regulatory sites in the tail of fungal conventional kinesin. *Nat. Cell. Biol.* **2**, 333 (2000).
13. Block, S.M., Nanometers and piconewtons - The macromolecular mechanics of kinesin. *Trends Cell Biol.* **5**, 169 (1995).
14. Kural, C., Kim, H., Syed, S., Goshima, G., Gelfand, V.I., and Selvin, P.R., Kinesin and dynein move a peroxisome in vivo: A tug-of-war or coordinated movement? *Science* **308**, 1469 (2005).
15. Romberg, L., Pierce, D.W., and Vale, R.D., Role of the kinesin neck region in processive microtubule-based motility. *J. Cell Biol.* **140**, 1407 (1998).
16. Caudron, N., Valiron, O., Usson, Y., Valiron, P., and Job, D., A reassessment of the factors affecting microtubule assembly and disassembly in vitro. *J. Mol. Biol.* **297**, 211 (2000).
17. Vorobiev, I., Malikov, V., and Rodionov, V., Self-organization of a radial microtubule array by dynein-dependent nucleation of microtubules. *Proc. Natl. Acad. Sci. U. S. A.* **98**, 10160 (2001).
18. Goel, A. and Vogel, V., Harnessing biological motors to engineer systems for nanoscale transport and assembly. *Nat. Nanotechnol.* **3**, 465 (2008).
19. Hess, H. and Bachand, G., Biomolecular motors. *Mater. Today* **8**, 22 (2005).
20. Hess, H., Bachand, G.D., and Vogel, V., Powering nanodevices with biomolecular motors. *Chem. Eur. J.* **10**, 2110 (2004).
21. van den Heuvel, M.G.L. and Dekker, C., Motor proteins at work for nanotechnology. *Science* **317**, 333 (2007).
22. Clemmens, J., Hess, H., Doot, R., Matzke, C.M., Bachand, G.D., and Vogel, V., Motor-protein roundabouts : Microtubules moving on kinesin-coated tracks through engineered networks. *Lab Chip* **4**, 83 (2004).
23. Clemmens, J., Hess, H., Howard, J., and Vogel, V., Analysis of microtubule guidance in open microfabricated channels coated with the motor protein kinesin. *Langmuir* **19**, 1738 (2003).
24. Clemmens, J., Hess, H., Lipscomb, R., Hanein, Y., Böhringer, K.F., Matzke, C.M., Bachand, G.D., Bunker, B.C., and Vogel, V., Mechanisms of microtubule guiding on microfabricated kinesin-coated surfaces: Chemical and topographic surface patterns. *Langmuir* **19**, 10967 (2003).
25. Hess, H., Clemmens, J., Matzke, C.M., Bachand, G.D., Bunker, B.C., and Vogel, V., Ratchet patterns sort molecular shuttles. *Appl. Phys. A* **75**, 309 (2002).
26. Hess, H., Matzke, C.M., Doot, R., Clemmens, J., Bachand, G.D., Bunker, B.C., and Vogel, V., Molecular shuttles operating undercover: A new photolithographic approach for the fabrication of structured surfaces supporting directed motility. *Nano Lett.* **3**, 1651 (2003).
27. Hiratsuka, Y., Tada, T., Oiwa, K., Kanayama, T., and Uyeda, T.Q.P., Controlling the direction of kinesin-driven microtubule movements along microlithographic tracks. *Biophys. J.* **81**, 1555 (2001).

28. Bachand, G.D., Rivera, S.B., Boal, A.K., Gaudioso, J., Liu, J., and Bunker, B.C., Assembly and transport of nanocrystal CdSe quantum dot nanocomposites using microtubules and kinesin motor proteins. *Nano Lett.* **4**, 817 (2004).

29. Brunner, C., Wahnes, C., and Vogel, V., Cargo pick-up from engineered loading stations by kinesin driven molecular shuttles. *Lab Chip* **7**, 1263 (2007).

30. Hutchins, B.M., Platt, M., Hancock, W.O., and Williams, M.E., Motility of CoFe2O4 nanoparticle-labelled microtubules in magnetic fields. *Micro Nano Lett.* **1**, 47 (2006).

31. Bachand, M., Trent, A., Bunker, B., and Bachand, G., Physical factors affecting kinesin-based transport of synthetic nanoparticle cargo. *J. Nanosci. Nanotech.* **5**, 718 (2005).

32. Boal, A., Bachand, G., Rivera, S., and Bunker, B., Interactions between cargo-carrying bio-molecular shuttles. *Nanotechnology* **17**, 349 (2006).

33. Bachand, G., Rivera, S., Carroll-Portillo, A., Hess, H., and Bachand, M., Active capture and transport of virus particles using a biomolecular motor-driven, nanoscale antibody sandwich assay. *Small* **2**, 381 (2006).

34. Soto, C.M., Martin, B.D., Sapsford, K.E., Blum, A.S., and Ratna, B.R., Toward single molecule detection of staphylococcal enterotoxin B: Mobile sandwich immunoassay on gliding microtabules. *Anal. Chem.* **80**, 5433 (2008).

35. Yokokawa, R., Miwa, J., Tarhan, M.C., Fujita, H., and Kasahara, M., DNA molecule manipulation by motor proteins for analysis at the single-molecule level. *Anal. Bioanal. Chem.* **391**, 2735 (2008).

36. Yokokawa, R., Tarhan, M.C., Kon, T., and Fujita, H., Simultaneous and bidirectional transport of kinesin-coated microspheres and dynein-coated microspheres on polarity-oriented microtubules. *Biotechnol. Bioeng.* **101**, 1 (2008).

37. Diez, S., Reuther, C., Dinu, C., Seidel, R., Mertig, M., Pompe, W., and Howard, J., Stretching and transporting DNA molecules using motor proteins. *Nano Lett.* **3**, 1251 (2003).

38. Dinu, C.Z., Opitz, J., Pompe, W., Howard, J., Mertig, M., and Diez, S., Parallel manipulation of bifunctional DNA molecules on structured surfaces using kinesin-driven microtubules. *Small* **2**, 1090 (2006).

39. Ramachandran, S., Ernst, K.-H., Bachand, G., Vogel, V., and Hess, H., Selective loading of kinesin-powered molecular shuttles with protein cargo and its application to biosensing. *Small* **2**, 330 (2006).

40. Liu, H., Spoerke, E.D., Bachand, M., Koch, S.J., Bunker, B.C., and Bachand, G.D., Biomolecular motor-powered self-assembly of dissipative nanocomposite rings. *Adv. Mater.* **17**, in press (2008).

41. Marte, B., Vaccinia virus on the move. *Nat. Rev. Mol. Cell Biol.* **2**, 792 (2001).

42. Moss, B. and Ward, B., High-speed mass transit for poxviruses on microtubules. *Nat. Cell Biol.* **3**, E245 (2001).

43. Suikkanen, S., Aaltonen, T., Nevalainen, M., Valilehto, O., Lindholm, L., Vuento, M., and Vihinen-Ranta, M., Exploitation of microtubule cytoskeleton and dynein during parvoviral traffic toward the nucleus. *J. Virol.* **77**, 10270 (2003).

44. Bearer, E.L., Breakefield, X.O., Schuback, D., Reese, T.S., and LaVail, J.H., Retrograde axonal transport of herpes simplex virus: Evidence for a single mechanism and a role for tegument. *Proc. Natl. Acad. Sci. USA* **97**, 8146 (2000).

45. Ward, B.M., The longest micron; transporting poxviruses out of the cell. *Cell. Microbiol.* **7**, 1531 (2005).

46. Coy, D.L., Wagenbach, M., and Howard, J., Kinesin takes one 8-nm step for each ATP that it hydrolyzes. *J. Biol. Chem.* **274**, 3667 (1999).

47. Limberis, L. and Stewart, R.J., Toward kinesin-powered microdevices. *Nanotechnology* **11**, 47 (2000).

48. Muthukrishnan, G., Hutchins, B.M., Williams, M.E., and Hancock, W.O., Transport of semiconductor nanocrystals by kinesin molecular motors. *Small* **2**, 626 (2006).

49. Beeg, J., Klumpp, S., Dimova, R., Gracia, R.S., Unger, E., and Lipowsky, R., Transport of beads by several kinesin motors. *Biophys. J.* **94**, 532 (2008).

50. Courty, S., Luccardini, C., Bellaiche, Y., Cappello, G., and Dahan, M., Tracking individual kinesin motors in living cells using single quantum-dot imaging. *Nano Lett.* **6**, 1491 (2006).

Distribution (electronics copies)

1	MS 0123 Donna Chavez, LDRD Office	1011
1	MS 0899 Technical Library	9536
1	MS 1413 Grant S. Heffelfinger	8630
1	MS 9054 Glenn D. Kubiak	8600
1	MS 1303 George D. Bachand	1132
1	MS 1303 Marlene Bachand	1132
1	MS 1303 Adrienne C. Greene	1132
1	MS 1411 Bruce C. Bunker	1816
1	MS 1411 Erik D. Spoerke	1816